



# CHORUS

This is the accepted manuscript made available via CHORUS. The article has been published as:

## Thermal Transport in Single-Walled Carbon Nanotubes Under Pure Bending

Jihong Ma, Yuxiang Ni, Sebastian Volz, and Traian Dumitrică

Phys. Rev. Applied **3**, 024014 — Published 25 February 2015

DOI: [10.1103/PhysRevApplied.3.024014](https://doi.org/10.1103/PhysRevApplied.3.024014)

## Thermal Transport in Single Wall Carbon Nanotubes under Pure Bending

Jihong Ma<sup>1)</sup>, Yuxiang Ni<sup>1)</sup>, Sebastian Volz<sup>2)</sup>, and Traian Dumitrică<sup>1, a)</sup>

<sup>1</sup>*Department of Mechanical Engineering, University of Minnesota, 111 Church Street SE, Minneapolis, MN 55455, USA*

<sup>2</sup>*Laboratoire d’Énergétique Moléculaire et Macroscopique, CNRS UPR 288, Ecole Centrale Paris, Grande Voie des Vignes, 92295 Châtenay-Malabry, France*

The carbon nanotubes’ resilience to mechanical deformation is a potentially important feature for imparting tunable properties at the nanoscale. Using non-equilibrium molecular dynamics and empirical interatomic potentials, we examine the thermal conductivity variations with bending in the thermal transport regime where both ballistic and diffusive effects coexist. These simulations are enabled by the realistic atomic-scale descriptions of uniformly curved and buckled nanotube morphologies obtained by imposing objective boundary conditions. We uncover a contrasting behavior. At shorter lengths, the phonon propagation is affected significantly by the occurrence of localized structural buckling. As the nanotube length becomes comparable with the phonon mean free path, heat transport becomes insensitive to the buckling deformations. Our result settles the controversy around the current differences between the current experimental and molecular dynamics measurements of the thermal transport in bent nanotubes.

## I. INTRODUCTION

The combination of extremely high thermal conductivity<sup>1-6</sup> and exceptional mechanical properties<sup>7-14</sup> of carbon nanotubes (CNTs) motivated the usage of this material for developing a variety of applications, including multifunctional materials<sup>15, 16</sup>, thermal switches and thermal interface materials<sup>17-20</sup>. The relation between the thermal transport and the bending deformation modes of single wall carbon nanotubes (SWCNTs) has not been yet established. When a SWCNT bends, it does not break. Instead, the strain energy is lowered by the formation of a structural kink<sup>8, 21-24</sup>. The potential effects of bending and buckling are important for the fundamental understandings of phonon scattering mechanisms in quasi-one dimensional

structures as well as for applications.

The thermal conductivity of stress free SWCNTs extends from ballistic to diffusive throughout a range of temperature and diameter-dependent lengths<sup>4</sup>. We are concerned with the thermal conductance regime exhibited by SWCNTs with lengths ( $l$ ) less than the phonon mean free path ( $l_{mfp}$ ). In this regime, atomistic molecular dynamics (MD) simulations<sup>6, 22, 23</sup> performed on SWCNTs up to hundreds of nanometers in length obtained that the thermal conductivity increases with length. The increase demonstrates the substantial contributions to thermal transport of the additional long-wavelength phonons created by increasing the SWCNT length<sup>25</sup>.

The mechanics of CNT bending is well understood and there is good quantitative agreement between theory and experimentation. For example, the observed critical strains for wavelike rippling<sup>22</sup> of multi-walled CNTs are only within few percent to the modeling predictions<sup>21, 24</sup>. In contrast, in the thermal domain not a uniform conclusion has been reached even qualitatively. Experiments<sup>26, 27</sup> uncovered robustness of heat transport along bent CNTs in both the diffusive and the ballistic regimes. In contrast, theoretical studies<sup>28-31</sup> considering the ballistic regime have revealed that bending and buckling cause thermal conductivity reductions.

There could be several reasons for the discrepancy between the experimental and theoretical results. A first explanation suggests that thermal conductivity reductions could be related to the challenges in simulating a bent SWCNT at the atomistic level. Indeed, the standard MD formulation under periodic boundary conditions is unusable since bending is incompatible with translational symmetry. For this reason, workers often make recourse to finite-size cluster representations, by considering SWCNTs as long as 50 nm. A bending deformation is usually imposed by rotating to a target angle the two rigid ends. Beside the disadvantage of introducing spurious effects, the procedure leads to deformed nanotubes with small bending portions (typically 8-nm long) and large straight ends<sup>30</sup>. Such morphologies are not similar with the ones

investigated in experiment<sup>27</sup>, where the bent portions are approaching the mean free path of the SWCNT. A related explanation brings up the observed diameter and length dependence for the onset of buckling<sup>21</sup>. The condition for buckling is fulfilled earlier in longer and large diameter SWCNTs. If thermal transport is strongly influenced by bending, only large diameter SWCNTs might exhibit robust thermal transport since less geometrical curvature and strain effect are needed to develop buckling. A final explanation invokes the differences in SWCNT length considered in experiment and current MD simulations. While experiments are probing the ballistic regime near its upper limit, simulations are considering tube lengths  $l$  well below  $l_{mfp}$ . The SWCNT length limits the longest possible phonon wavelength that can exist. The origin of the discrepancy may originate in the contribution of the low-frequency phonons that are not accounted for in the MD simulations considering short tubes. We find that the conjuncture of the first and last explanations to be correct. By increasing the lengths of the considered bent SWCNTs closer to  $l_{mfp}$ , our MD simulations predict that thermal transport becomes insensitive to the buckling deformation.

## II. COMPUTATIONAL METHODS

To simulate realistically bent SWCNTs we employ the generalization of periodic MD termed objective MD<sup>32-34</sup>. With this method, the whole simulated SWCNT is in pure bending, which represents a condition of stress where only a bending moment is applied. Our objective boundary conditions write

$$\mathbf{r}_{i,\zeta} = \mathbf{R}^\zeta \mathbf{r}_i \quad i = 1, 2, \dots, N. \quad (1)$$

Here  $N$  is the total number of atoms located at positions  $\mathbf{r}_i$  located in the primary cell.  $\mathbf{r}_{i,\zeta}$  are the positions of the corresponding atoms in the image cell indexed by  $\zeta$  and  $\mathbf{R}$  denotes the applied rotation of angle  $\theta$  performed around the  $z$  axis, which is the rotation axis. As  $\theta$  is the only constraint imposed here, the atoms are free to move away or towards the rotational axis. The

curvature  $\tau$  of the SWCNT, then, is not imposed but it is the result of the energy minimization. By varying  $\theta$ , we are able to generate bent SWCNTs with different curvatures. For example, Fig. 1 (a) shows a bent morphology of a (10,10) SWCNT supercell with  $l=30.75$  nm containing 5,000 carbon atoms. The bending angle is  $\theta = 60^\circ$  and the shape of the relaxed bent tube is nicely smooth. The curvature, defined as  $\tau = \theta/l$ , is everywhere  $0.106 \text{ nm}^{-1}$ .

In an earlier work<sup>21</sup>, we have demonstrated that, in spite of the imposed objective periodicity, objective MD is able to describe the expected localized buckling of SWCNTs and all related essential details, including the scaling with diameter and length of the critical curvature beyond which SWCNTs behave nonlinearly. Building on this work, which considered SWCNT supercells up to 16 nm in lengths, here we report that the method can capture bending and localized kinking of much larger SWCNT portions. Referring to Fig. 1, as we further increased  $\theta$ , a single kink developed as shown in Fig. 1(b) for  $\theta = 77.14^\circ$ . Using this approach, we have built a collection of bent structures comprising (10,10) and (6,6) SWCNTs up to 90 nm in length.

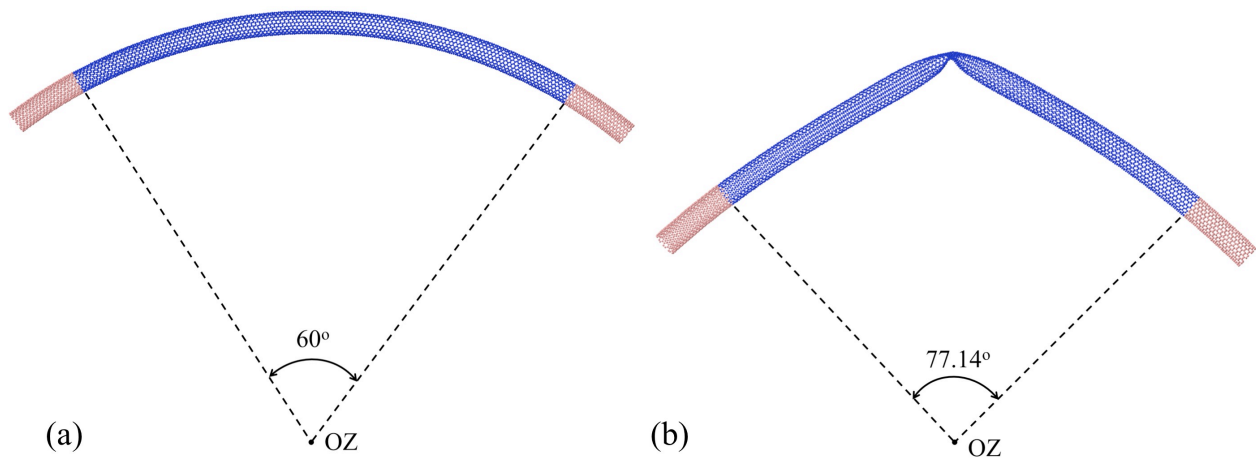


FIG. 1. Objective MD configurations of a (10,10) SWCNT bent (a) without and (b) with a kink. The atoms located inside the simulation cell are represented in dark gray (blue). Atoms in the  $\zeta = -1$  and  $\zeta = 1$  image cells are showed in light gray (pink). The measured curvatures are (a)  $0.034 \text{ nm}^{-1}$  and (b)  $0.044 \text{ nm}^{-1}$ .

Relying on the objective bent morphologies, we have performed non-equilibrium molecular dynamics (NEMD) simulations<sup>35</sup> to understand the thermal transport. The interatomic interactions were described with the AIREBO potential<sup>36</sup>, which includes a Lennard-Jones term describing the van der Waals interactions experienced by the C-C atoms located in the 2-10.2 Å space interval. The non-bonded interactions at the kink should manifest into an increase of the phonon scattering rate. The proposed NEMD simulation set-up is shown in Fig. 2(a) for a (10,10) SWCNT. One unit cell at each end was fixed in order to impose the bending constraints. Such a small size is sufficient in view of the short range of the potential. Four other unit cells next to each end were set as the hot and cold heat baths, respectively. In order to minimize the thermal boundary resistance effect, the length of the bath regions was increased in the subsequent calculations involving (10,10) SWCNTs. We used six unit cells for  $l \leq 55.4$  nm, twelve unit cells for  $l = 65.2$  nm, and eighteen unit cells for  $l = 90$  nm. The time step used in NEMD simulations was 0.5 fs. Initially, the whole dynamic system was equilibrated at 300 K with the help of a Nose-Hoover thermostat. Next, the temperatures of the two heat baths were rescaled at every time step to maintain  $T_h=310$  K and  $T_c=290$  K, respectively. The velocity Verlet algorithm was used for time integration. Steady-state has been reached after 1,000 ps. The rate of kinetic energy exchange between the two baths was obtained as

$$Q = \frac{1}{2} \langle Q_h - Q_c \rangle. \quad (2)$$

Here  $Q_h$  and  $Q_c$  are the instantaneous heat currents flowing into and away the hot and cold baths to maintain the temperature gradient.  $Q_h - Q_c$  equals the difference in instantaneous kinetic energies of the atoms located in the hot and cold bath regions. The angle brackets indicate a statistical average, taken here over the last 5,000 ps after the steady state was reached. The thermal conductivity is then calculated as

$$\kappa = q \left( \frac{dT}{dx} \right)^{-1} \quad (3)$$

where  $q$  is the heat current per cross-sectional area  $A$  and  $x$  is the axial position. We defined  $A$  by assuming a 0.34 nm thickness for a one-atom thick tube wall. The local temperature  $T$  is computed by statistically averaging the kinetic energy of the atoms located on three subsequent unit cells.

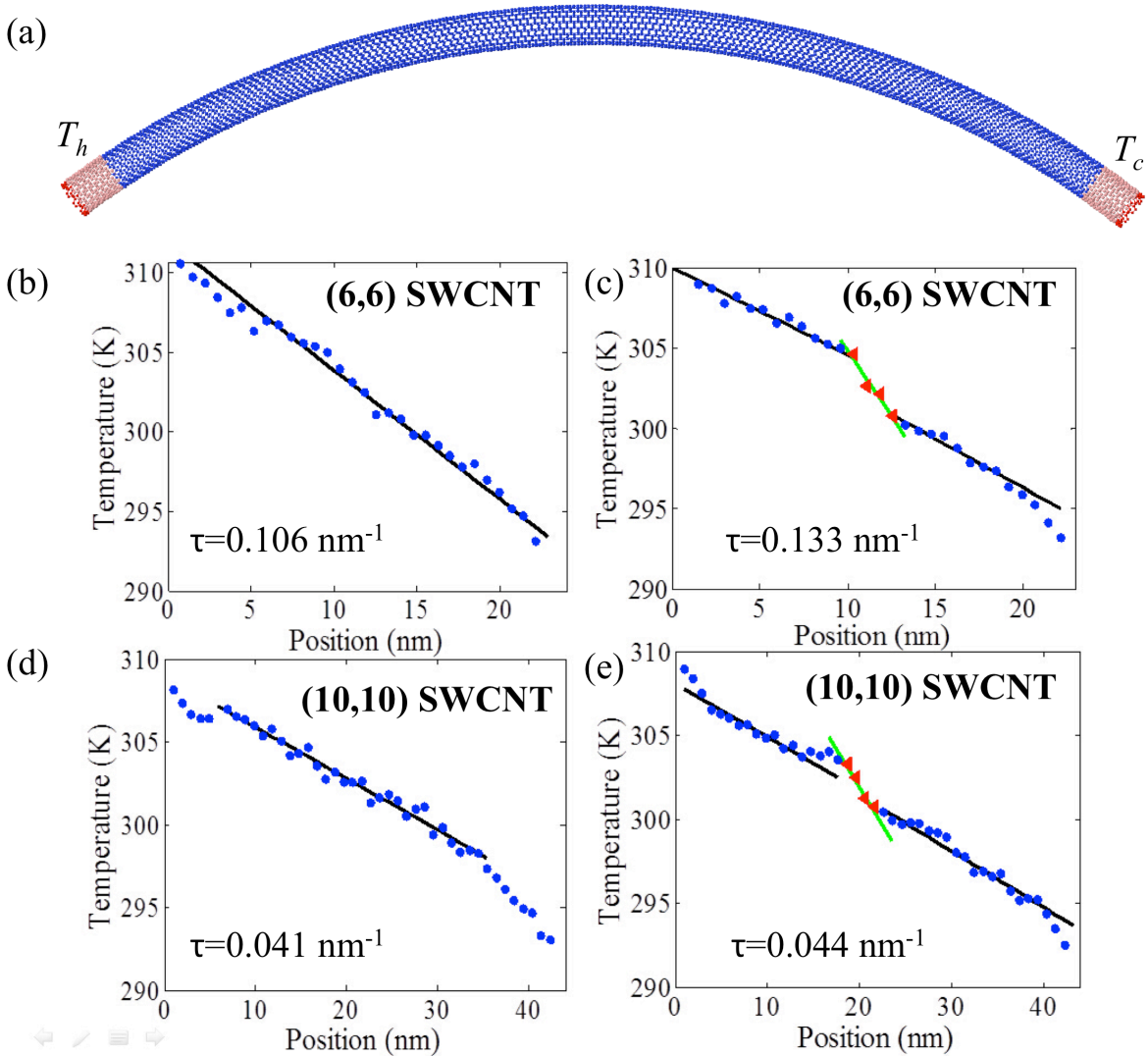


FIG 2. (a) Set-up for the NEMD simulation with uni-directional flux. Temperature profiles in bent (6,6) SWCNT (b) ideal (unkinked) and (c) kinked. The total length is 24.6 nm. Temperature profiles in a bent (10,10) SWCNT with (d) ideal (unkinked) and (e) kinked structure. The total length is 45.5 nm. Circles are the local temperatures of the unkinked regions. The red triangles in (c) and (e) represent the temperature in the kink region. Fitted lines are shown in all figures.

### III. RESULTS AND DISCUSSION

We first examine short (in comparison with  $l_{mfp}$ ) SWCNTs before and after their buckling threshold. We considered SWCNTs with different diameters and lengths to provide an opportunity to probe different curvature regimes. Panels (b-e) of Fig. 2 display the obtained temperature profiles along the nanotube length for selected curvatures. For the unkinked cases, we extracted the thermal conductivity by considering the temperature gradient observed in the linear region. We excluded the temperature points from the regime near the thermal baths, since these points are largely affected by the undesirable effect of phonon scattering at the interfaces between thermostatted and non-thermostatted regions. For both SWCNTs, we obtained that the central kink is associated with a pronounced thermal gradient over a length  $l_k$ . Unlike the interface effect mentioned above, the thermal resistance at the kink is a real effect. We accounted for it with a series model, where the overall conductivity writes

$$\frac{1}{\kappa} = \frac{(1 - \phi)}{\kappa_i} + \frac{\phi}{\kappa_k}. \quad (4)$$

Here  $\kappa_i$  and  $\kappa_k$  denote the local thermal conductivities obtained from the slopes identified in the unkinked and kinked regions.  $\phi = l_k/l$  is the length fraction of the kinked region. The above model is appropriate since there is no direct interactions between the two SWCNT sections around the kink. There is only one path for the heat flux, through the kink.

Table 1 summarizes our simulation results at all considered curvatures. The overall thermal conductivity values entered in the last column demonstrate that the conductivity reduction occurs in a gradual manner and that the reduction is small for both nanotubes. By the time the (6,6) SWCNT develops buckling, we measured a 44% decrease in  $\kappa$  with respect to the zero-curvature reference case. For the longer and larger diameter (10,10) SWCNTs the reduction is of 20%, which is still significant. (The difference in values reflects the smaller critical

curvature for buckling in larger diameter SWCNT.) We also see that at the kink location the local thermal conductivity differs significantly from the rest of the tube. For both nanotubes  $\kappa_k$  is about 36% of the unknicked region. For a more transparent characterization of the kink, we estimate the equivalent length of a pristine SWCNT that would give a similar effect. This equivalent length was calculated as  $l_k \kappa_o / \kappa_k$ , where  $\kappa_o$  is the pristine thermal conductivity. For the (10,10) CNTs, we find equivalent lengths of 11.90 and 20.27 nm, for  $\tau$  of and  $0.044 \text{ nm}^{-1}$  and  $0.047 \text{ nm}^{-1}$ , respectively. Interestingly, these values are larger than the 9 nm value reported for kinks formed under 6% compressive strain<sup>31</sup>.

Structure			$\kappa_i$ (W/mK)	$\kappa_k$ (W/mK)	$\frac{\kappa_k}{\kappa_i}$	$\phi$	$\kappa$ (W/mK)
SWCNT	$l$ (nm)	$\tau$ ( $\text{nm}^{-1}$ )					
(6,6)	24.6	0.000	-				120.7
		0.106	-				89.2
		0.133	83.7	29.9	35.7%	13%	67.5
(10,10)	45.5	0.000	-				155.8
		0.034	-				154.5
		0.041	-				146.4
		0.044	143.2	51.5	36.0%	8.7%	124.1
		0.047	141.4	30.2	21.4%	8.7%	107.1

TABLE 1. Thermal conductivities of bent (6,6) and (10,10) SWNTs with  $l$  much smaller than  $l_{mfp}$ . The straight case is shown for a comparison.

The thermal resistance at the kink is attributed to the local strain. To gain more insight into the underlying microscopic mechanism, we have analyzed the local phonon density of states (LPDOS) around the kink and the corresponding region of the unknicked and straight (10,10) SWCNT structures. LPDOS was obtained by decomposing into the Fourier space the MD time correlation function of the atomic velocities at 300 K. Fig. 3 reveals major differences only for the optical G-mode phonons with frequencies around 52 to 54.2 THz (as described with the AIREBO potential<sup>37</sup>). It could be expected that a bending strain affects the G-modes since they correspond to the C-C bond-stretching motion. We see that as  $\tau$  increases, the G peak is lowered, broadened, and then split into two peaks. The shift to lower (higher) frequencies corresponds to

a decrease (increase) of the force constants for the C-C bonds elongated (compressed) under the bending deformation. The broadening allows for the optic phonons to provide more scattering channels for the heat carrying acoustic modes through Umklapp scattering especially in the acoustic-acoustic-optic scattering, where the sum of two acoustic frequencies must equal the optic frequency. Thus, we conjecture that the MD-computed  $\kappa$  lowering with increasing  $\tau$  could originate in the G-band broadening.

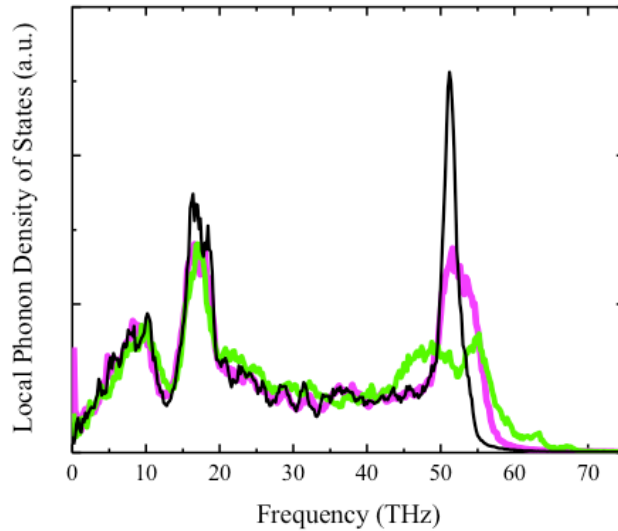


FIG 3. LPDOS in a 45.5 nm long (10,10) SWCNT as a function of frequency, for straight - black line, unkinked bent with  $\tau=0.034 \text{ nm}^{-1}$  - magenta (gray continuous thick) line, and kinked bent with  $\tau=0.047 \text{ nm}^{-1}$  - green (light gray continuous thin) line. LPDOS is calculated over a portion comprising 9 unit cells.

We now examine the consequences of increasing  $l$  in order to probe the explanation which attributes the thermal conductivity robustness to the additional low-frequency acoustic phonons that emerge as  $l \sim l_{mfp}$ . In Fig. 4 we compare the size dependence of  $\kappa$  for a (10,10) SWCNT in the straight and bent with  $\tau=0.034 \text{ nm}^{-1}$  and  $\tau=0.047 \text{ nm}^{-1}$  states. Relying on the recent detailed investigations<sup>38</sup>, we have adopted the view that in NEMD simulations with unidirectional heat flux, the whole SWCNT length determines thermal conductivity. Thus, in Fig. 4 we have plotted  $\kappa$  against  $l$ , which comprises the heat bath regions. We see that as the sample

length increases, the maximum allowable phonon wavelength increases. For the stress-free tubes, we attribute the  $\kappa$  increase with length to effective contribution of the long-wavelength phonons. We also see that there is no distinction in the conductivity variations of the straight and ideally bent states, suggesting that the transport in ideally bent SWCNTs is ballistic, as in the stress-free case. Finally, our data demonstrate that the impact of the kink diminishes quickly as  $l$  increases. While for  $l=24.8$  nm  $\kappa$  differs by 38% from the ideal straight state, at  $l=90$  nm the difference reduces to only 5.7%. Thus, our simulations confirm the robustness of the thermal transport observed in experiments. Note that our MD calculated thermal conductivities did not include quantum effects. The quantum corrected  $\kappa$  are estimated<sup>39</sup> as 84% of those presented in Fig. 4. The quantum-corrected temperature is 260 K when the MD temperature is 300 K.

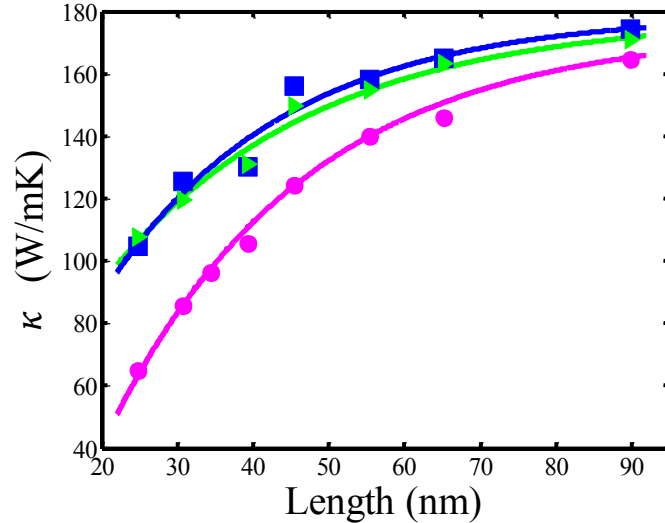


FIG 4. Thermal conductivity in a (10,10) SWCNT as a function of the sample length, for straight – blue (dark gray) squares, bent (unkinked) with  $\tau=0.034$  nm<sup>-1</sup> – green (light gray) triangles, and bent (kinked) with  $\tau=0.044$  nm<sup>-1</sup> - magenta (gray) circles. Lines represent exponential fitting of the length dependence.

#### IV. CONCLUSIONS

Enabled by the bent morphologies calculated under objective boundary conditions, we studied for the first time the effect of pure bending strain on the thermal transport of SWCNT

with different sizes. NEMD simulations revealed that the kink developed under bending exhibits a much larger resistance related effective length than previously suggested. In the short  $l$  regime, the overall  $\kappa$  exhibits a sizable decrease by the time buckling occurs. The  $\kappa$  reduction is most significant in small diameter SWCNTs, which display a higher critical curvature for buckling. The finding is important since significant tunability of the thermal conductivity characteristic for the  $l \ll l_{mfp}$  regime is interesting for applications. As  $l \sim l_{mfp}$  thermal conductivity becomes robust as the heat carrying long-wavelength phonons become insensitive to the localized buckling deformation.

## ACKNOWLEDGEMENTS

We acknowledge support from NSF CMMI-1332228. Computations were performed using resources from the Minnesota Supercomputing Institute and XSEDE.

---

<sup>a)</sup>Electronic mail: [dtraian@umn.edu](mailto:dtraian@umn.edu)

## REFERENCES

1. J. Che, T. Çagin and W. A. G. III, Thermal conductivity of carbon nanotubes. *Nanotechnol.* **11**, 65 (2000).
2. M. Fujii, X. Zhang, H. Xie, H. Ago, K. Takahashi, T. Ikuta, H. Abe and T. Shimizu, Measuring the thermal conductivity of a single carbon nanotube. *Phys. Rev. B* **96**, 065502 (2005).
3. N. Mingo and D. A. Broido, Carbon nanotube ballistic thermal conductance and its limits. *Phys. Rev. Lett.* **95**, 096105 (2005).
4. N. Mingo and D. A. Broido, Length dependence of carbon nanotube thermal conductivity and the “Problem of Long Waves”. *Nano Lett.* **5**, 1221 (2005).
5. E. Pop, D. Mann, Q. Wang, K. Goodson and H. Dai, Thermal conductance of an individual single-wall carbon nanotube above room temperature. *Nano Lett.* **6**, 96 (2006).
6. J. Shiomi and S. Maruyama, Molecular dynamics of diffusive-ballistic heat conduction in single-walled carbon nanotubes. *Jpn. J. Appl. Phys.* **47**, 2005 (2008).
7. M. R. Falvo, G. J. Clary, R. M. Taylor, V. Chi, F. P. Brooks, S. Washburn and R. Superfine, Bending and buckling of carbon nanotubes under large strain. *Nature* **389**, 582 (1997).
8. S. Iijima, C. Brabec, A. Maiti and J. Bernholc, Structural flexibility of carbon nanotubes. *J. Chem. Phys.* **104**, 2089 (1996).
9. E. Hernandez, C. Goze, P. Bernier and A. Rubio, Elastic properties of C and B<sub>x</sub>C<sub>y</sub>N<sub>z</sub> composite nanotubes. *Phy. Rev. Lett.* **80**, 4502 (1998).

10. B. G. Demczyk, Y. M. Wang, J. Cumings, M. Hetman, W. Han, A. Zettl and R. O. Ritchie, Direct mechanical measurement of the tensile strength and elastic modulus of multiwalled carbon nanotubes. *Mater. Sci. Eng. A* **334**, 173 (2002).
11. T. Dumitrică, M. Hua and B. I. Yakobson, Symmetry-, time-, and temperature-dependent strength of carbon nanotubes. *Proc. Natl. Acad. Sci. USA* **103** ( ), 6105 (2006).
12. D.-B. Zhang and T. Dumitrică, Elasticity of ideal single-walled carbon nanotubes via symmetry-adapted tight-binding objective modeling. *Appl. Phys. Lett.* **93**, 031919 (2008).
13. D.-B. Zhang, R. D. James and T. Dumitrică, Electromechanical characterization of carbon nanotubes in torsion via symmetry-adapted tight-binding objective molecular dynamics. *Phys. Rev. B* **80**, 115418 (2009).
14. Q. Wang, K. M. Liew and W. H. Duan, Modeling of the mechanical instability of carbon nanotubes. *Carbon* **46**, 285 (2008).
15. J. M. Harris, G. R. S. Iyer, A. K. Bernhardt, J. Y. Huh, S. D. Hudson, J. A. Fagan and E. K. Hobbie, Electronic durability of flexible transparent films from type-specific single-wall carbon nanotubes. *ACS Nano* **6**, 881 (2012).
16. P. P. S. S. Abadi, M. R. Maschmann, R. Matthew, S. M. Mortuza, S. Banerjee, J. W. Baur, S. Graham and B. A. Cola, Reversible tailoring of mechanical properties of carbon nanotube forests by immersing in solvents. *Carbon* **69**, 178 (2014).
17. D. Fabris, P. Wilhite, C. Y. Yang, T. Yamada, M. Rosshirt and C. Cardenas, Application of carbon nanotubes to thermal interface materials. *J. Elect. Pack.* **133**, 020902 (2011).
18. B. A. Cola, X. Xu and T. S. Fisher, Increased real contact in thermal interfaces: a carbon nanotube/foil material. *Appl. Phys. Lett.* **90**, 093513 (2007).
19. M. Panzer, G. Zhang, D. Mann, X. Hu, E. Pop, H. Dai and K. E. Goodson, Thermal properties of metal-coated vertically aligned single-wall nanotube arrays. *ASME J. Heat Transf.* **130**, 052401 (2008).
20. Y. Ni, H. L. Khanh, Y. Chalopin, J. Bai, P. Lebarry, L. Divay and S. Volz, Highly efficient thermal glue for carbon nanotubes based on azide polymers. *Appl. Phys. Lett.* **100**, 193118 (2012).
21. I. Nikiforov, D.-B. Zhang, R. D. James and T. Dumitrică, Wavelike rippling in multi-walled carbon nanotubes under pure bending. *Appl. Phys. Lett.* **96**, 123107 (2010).
22. H. Jackman, P. Krakhmalev and K. Svensson, Measurements of the critical strain for rippling in carbon nanotubes. *Appl. Phys. Lett.* **98**, 183104 (2011).
23. P. C. Tsai, Y. R. Jeng, Y. X. Huang and K. T. Wu, Buckling characterizations of an individual multi-walled carbon nanotube: Insights from quantitative in situ transmission electron microscope nanoindentation and molecular dynamics. *Appl. Phys. Lett.* **103**, 053119 (103).
24. I. Arias and M. Arroyo, Size-dependent nonlinear elastic scaling of multiwalled carbon nanotubes. *Phys. Rev. Lett.* **100**, 085503 (2008).
25. A. Cao and J. Qu, Size dependent thermal conductivity of single-walled carbon nanotubes. *J. Appl. Phys.* **112**, 013503 (2012).
26. C. W. Chang, D. Okawa, H. Garcia, A. Majumdar and A. Zettl, Nanotube phonon waveguide. *Phys. Rev. Lett.* **99**, 045901 (2007).
27. V. Lee, R. Chen and C.-W. Chang, Probing the limit of one-dimensional heat transfer under extreme bending strain. *Phys. Rev. B* **87**, 035406 (2013).
28. F. Nishimura, T. Shiga, S. Maruyama, K. Watanabe and J. Shiomi, Thermal conductance of buckled carbon nanotubes. *Jpn. J. Appl. Phys.* **51**, 015102 (2012).

29. Z. Huang, Z. Tang, J. Yu and S. Bai, Temperature-dependent thermal conductivity of bent carbon nanotubes by molecular dynamics simulation. *J. Appl. Phys.* **109**, 104316 (2011).
30. A. N. Volkov, T. Shiga, D. Nicholson, J. Shiomi and L. V. Zhigilei, Effect of bending buckling of carbon nanotubes on thermal conductivity of carbon nanotube materials. *J. Appl. Phys.* **111**, 053501 (2012).
31. Z. P. Xu and M. J. Buehler, Strain controlled thermomutability of single-walled carbon nanotubes. *Nanotechnol.* **20**, 185701 (2009).
32. R. D. James, Objective structures. *J. Mech. Phys. Solids* **54**, 2354 (2006).
33. T. Dumitrică and R. D. James, Objective molecular dynamics. *J. Mech. Phys. Solids* **55**, 2206 (2007).
34. R. Rurali and E. Hernandez, Trocadero: a multiple-algorithm multiple-model atomistic simulation program. *Comp. Mat. Sci.* **28**, 85 (2003).
35. S. J. Plimpton, Fast parallel algorithms for short-range molecular dynamics. *J. Comp. Phys.* **117**, 1 (1995).
36. S. J. Stuart, A. B. Tutein and J. A. Harrison, A reactive potential for hydrocarbons with intermolecular interactions *J. Chem. Phys.* **112**, 6472 (2000).
37. Z.-Y. Ong, E. Pop and J. Shiomi, Reduction of phonon lifetimes and thermal conductivity of a carbon nanotube on amorphous silica. *Phys Rev. B* **84**, 165418 (2011).
38. R. N. Salaway and L. V. Zhigilei, Molecular dynamics simulations of thermal conductivity of carbon nanotubes: Resolving the effects of computational parameters. *Int. J. Heat Mass Transfer* **70**, 954 (2014).
39. J. R. Lukes and H. Zhong, Thermal conductivity of individual single-wall carbon nanotubes. *ASME J. Heat Transf.* **129**, 705 (2007).